

## Stronger Aramids through Molecular Design and Nanoprocessing

Amalia Rapakousiou,<sup>a</sup> Alejandro López-Moreno,<sup>a</sup> Belén Nieto-Ortega,<sup>a</sup> M. Mar Bernal,<sup>a</sup> Miguel A. Monclús,<sup>b</sup> Santiago Casado,<sup>a</sup> Cristina Navío,<sup>a</sup> Luisa R. González,<sup>c</sup> Juan P. Fernández-Blázquez,<sup>b</sup> Juan J. Vilatela,<sup>\*,b</sup> and Emilio M. Pérez<sup>\*,a</sup>

### SUPPORTING INFORMATION

#### Contents:

- 1) General data
- 2) General procedure for the synthesis of aramid oligomers **oPTA** and **oPyrTA**
- 3) Synthesis of N-pyrenylbenzamide **monoPyrTA**
- 4) <sup>1</sup>H NMR spectra of **oPTA** and **oPyrTA**
- 5) UV-vis spectra and emission spectra of **oPTA** and **oPyrTA**
- 6) TGA of **oPTA** and **oPyrTA**
- 7) Computational studies
- 8) Determination of the average molecular weight of **oPTA** and **oPyrTA** by intrinsic viscosity measurement
- 9) Determination of mass attenuation coefficient by UV-visible and estimation of number of oligomer units
- 10) Characterization of **monoPyrTA**
- 11) Synthesis of **oPyrTA** nanofibers
- 12) SEM images of **oPyrTA** nanofibers
- 13) Synthesis of **oPyrTA** nanofilms
- 14) Comparative FT-IR spectra of **monoPyrTA**, **oPyrTA** and **oPyrTA** nanofilms
- 15) Raman spectroscopy of **oPyrTA** nanofilms
- 16) TGA of **oPyrTA** nanofilms
- 17) SEM/EDS of **oPyrTA** nanofilms
- 18) UV/Vis. analysis of **oPyrTA** nanofilms
- 19) AFM of **oPyrTA** nanofilms
- 20) Nanoindentation measurements

## 1) General Data.

The NMR experiments were performed on a Bruker Avance 400 spectrometer (Magnet Ascend 400), operating at a frequency of 400 MHz and the  $^{13}\text{C}$  CP-MAS-NMR spectra were obtained with a Bruker AV 400 WB spectrometer.

Scanning electron microscopy (SEM) images were obtained with (Carl-Zeiss) SEM-EVO HD15 instrument with a detector SE operating at 1 kV- 3 kV. SEM/EDS mapping is recorded with a Bruker-Quantax model with detector X-Flash 400, coupled to the SEM-EVO HD15, operating at 30 kV with 1.09 kcps. The EDAX system has a resolution of 133 eV and an effective detection area of 30 mm<sup>2</sup>.

Fourier transform infrared (FT-IR) spectra were recorded on a FTIR Bruker IFS66v spectrometer. Products were pressed with KBr pellets.

UV-vis-NIR spectra of the solutions were obtained in an Agilent Cary 5000 UV-Vis-NIR spectrometer. Fluorescence spectra were obtained in a Horiba Jobin Yvon Fluorolog-4.

X-ray diffraction measurements were performed with an XRD Diffractometer Siemens D5000.

Raman spectra were acquired with a Bruker Senterra confocal Raman microscopy instrument, equipped with 532, 633 and 785 nm lasers.

Thermogravimetric analyses (TGA) were performed using a TA Instruments TGA Q500 with a ramp of 10 °C/min under air and nitrogen from 100 to 1000 °C.

For Nanoidentation measurements see details in p.p. S21-S23.

For Computational studies see details in p.p. S6

XPS (X ray Photoelectron Spectroscopy) measurements were performed under Ultra High Vacuum conditions (UHV, with a base pressure of  $7 \times 10^{-10}$  mbar), using a monochromatic Al K $\alpha$  line as exciting photon source for core level analysis ( $h\nu = 1486.7$  eV). The emitted photoelectrons were collected in a hemispherical energy analyzer (SPHERA-U7, pass energy set to 20 eV for the XPS measurements to have a resolution of 0.6 eV and to compensate the built up charge on the sample surface it was necessary (for the XPS measurements) the use of a Flood Gun (FG-500, Specs), with low energy electrons of 3 eV and 40  $\mu\text{A}$ .

AFM was performed in a JPK NanoWizard II<sup>®</sup> AFM, used in dynamic mode in air with a NT-MDT commercial silicon NSG01 cantilever tip (5.1 N/m and 150 kHz), with typical 6 nm radius at the end.

## 2) General procedure for the synthesis of aramid oligomers oPTA and oPyrTA

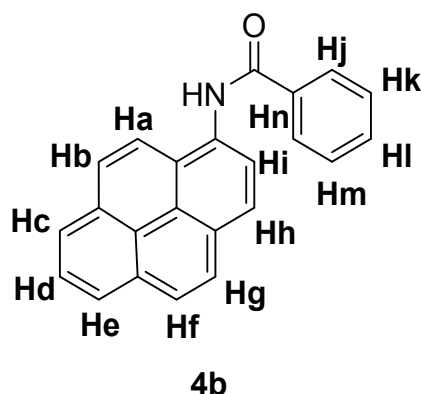
Synthesis of oligomer oPTA:

In an argon filled round bottom flask, 1.1 g (10 mmol) of finely grounded anhydrous calcium chloride was dissolved in 40 mL of N-methylpyrrolidone (NMP) and then 1 g (9.24 mmol) of p-phenylenediamine. Over the mixture, 1.86 mL (23 mmol) of pyridine were added and the flask was cooled to 0 °C. 1.87 g (9.24 mmol) of terephthaloyl chloride (TPC) was added in three portions maintaining the temperature below 10 °C. A gel was formed with the addition of TPC. After stirring for 1 hour the mixture was filtered through a 0.2 µm- pore size polycarbonate membrane and thoroughly washed with deionized water and methanol. 2.5 g of a yellowish solid was obtained. <sup>1</sup>H NMR spectra in D<sub>2</sub>SO<sub>4</sub> exhibits signals between 8 and 9 ppm. oligomer

Synthesis of oligomer oPyrTA:

oPyrTA was synthesized according to the above general procedure. 1 g of oPyrTA was synthesized from 530 mg (2.26 mmol) of 1,6-diaminopyrene, 458 mg (2.26 mmol) of terephthaloyl chloride, 260 mg (2,34 mmol) of anhydrous calcium chloride and 0.45 mL (5.57 mmol) of pyridine in 10 mL of NMP. Dark green solid was obtained. <sup>1</sup>H NMR spectra in D<sub>2</sub>SO<sub>4</sub> exhibits signals between 8.6 and 9.6 ppm.

## 3) Synthesis of N-pyrenylbenzamide monoPyrTA.



Synthesis of monoPyrTA:

To a stirred solution of 1,6 diaminopyrene (200 mg, 0.92 mmol) in 10 mL of THF, were added triethylamine (98 mg, 0.97 mmol) and benzoyl chloride (136 mg, 0.97 mmol) dropwise at 0°C. The reaction mixture was stirred at room temperature for 8 h. Then the mixture was filtered and evaporated. The solid (filtrate) was washed in pentane and extracted in EtOAc. The extract was washed three times with brine, dried with Na<sub>2</sub>SO<sub>4</sub> and evaporated under reduced pressure. Solid monoPyrTA was obtained in 80% yield (230 mg). <sup>1</sup>H NMR (400 MHz, DMSO) δppm 10.84 (s, 1H, -NH), 8.37 – 8.15 (m, 10H, Ha, Hb, Hc, He, Hf, Hg, Hh, Hi, Hj, Hn), 8.08 (t, *J* = 7.6 Hz, 1H, Hd), 7.67 – 7.57 (m, 3H, Hk, Hl, Hm). <sup>13</sup>C NMR (101 MHz, DMSO) δppm: 166.3 (-NHCO-), 134.5, 131.9, 131.8, 130.8, 130.5, 129.0, 128.5, 127.9, 127.2, 127.2, 126.9, 126.4, 125.7, 125.3, 125.2, 125.1, 124.9, 124.4, 123.8, 123.0 ppm.

#### 4) $^1\text{H}$ NMR spectra of **o**PTA and **o**PyrTA

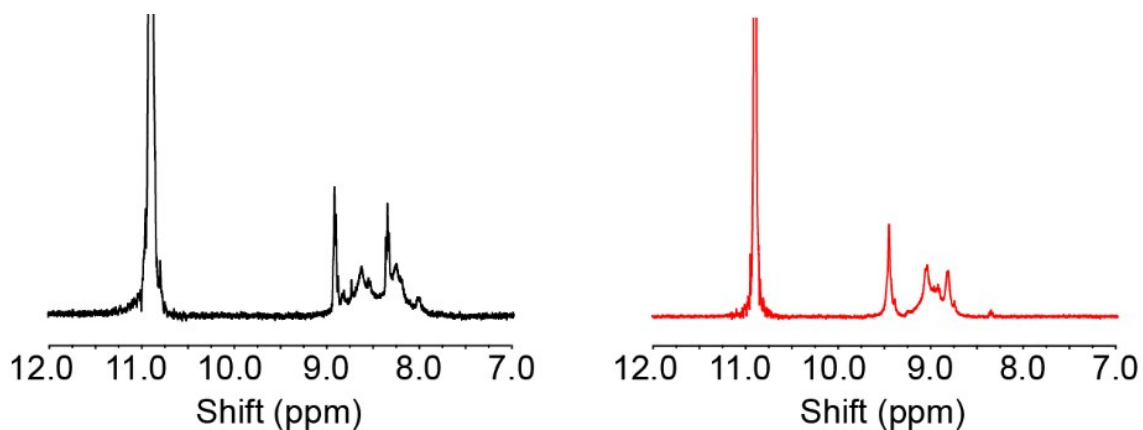


**Figure S1.** a)  $^1\text{H}$  NMR spectra in  $\text{D}_2\text{SO}_4$  at 25  $^\circ\text{C}$  of **o**PTA (black) and **o**PyrTA (red).

Figure S1 exhibits the  $^1\text{H}$ -NMR spectra of **o**PTA and **o**PyrTA in deuterated sulfuric acid. The spectra agree with the expected for both compound with a shift of 1 ppm between aromatic signals of pyrene unit of **o**PyrTA and the benzene ring of **o**PTA.

#### 5) UV-vis spectra and emission spectra of **o**PTA and **o**PyrTA.

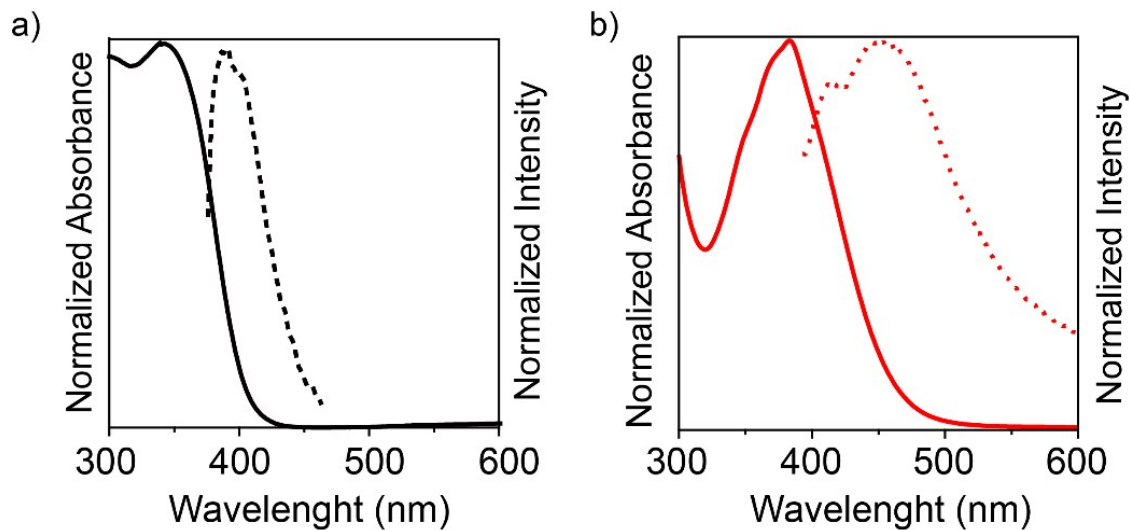


**Figure S2.** a) UV-vis spectra (black) and emission spectra (dashed black) of **o**PTA and b) UV-vis spectra (red) and emission spectra (dashed red) of **o**PyrTA.

6) TGA of oPTA and oPyrTA.

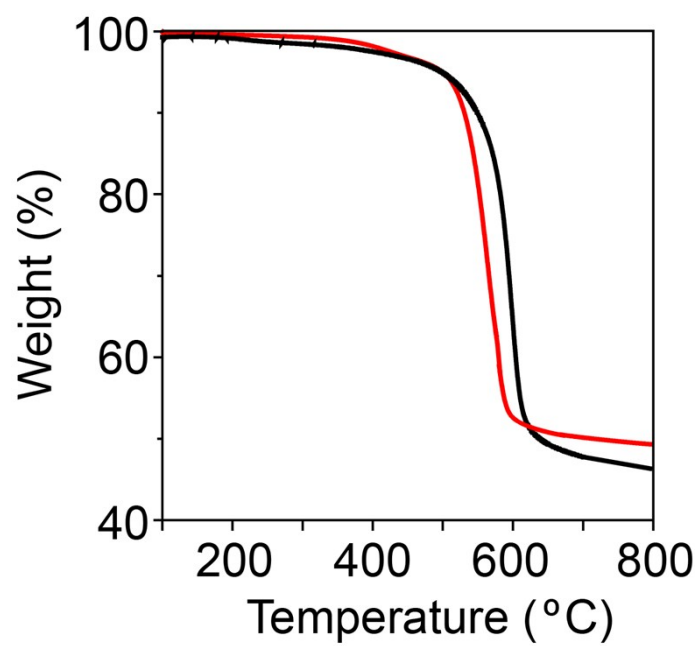
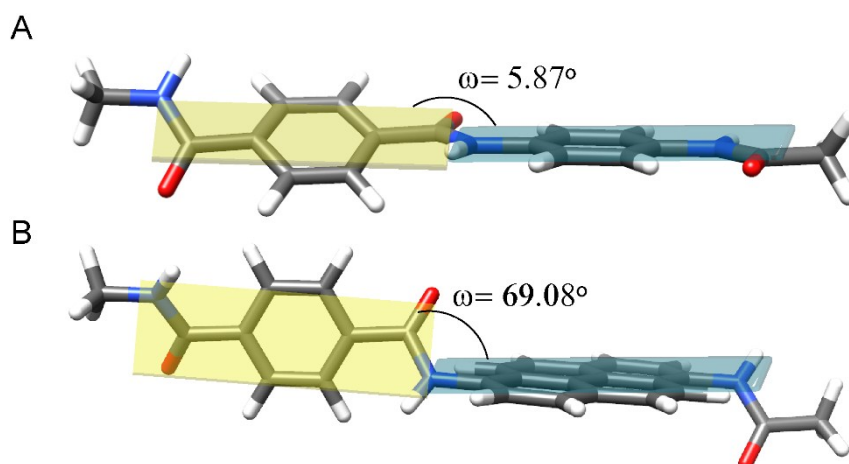


Figure S3. TGA analysis ( $N_2$ ,  $10^\circ C\ min^{-1}$ ) of oPTA (black) and oPyrTA (red)

## 7) Computational details

All theoretical DFT calculations were carried out within the density functional theory (DFT) approach by using the C.01 revision of the Gaussian 09 program package. Optimization and energy calculations were performed using the long-range corrected B97D density functional, which are able to incorporate the dispersion effects by means of a pair-wise London-type potential. The B97D density functional has emerged as a robust and powerful density functional able to provide accurate structures in large supramolecular aggregates dominated by non-covalent interactions of different nature with the minimum computational time. The widely used Becke's threeparameter B3LYP functional is not adequate to calculate the formation of supramolecular aggregates because it fails in describing dispersion forces and does not properly account for stacking  $\pi$ - $\pi$  interactions. The B97D functional was combined with Pople's 6-31G(d,p) basis set.

The geometry of the isolated monomers **oPTA** and **oPyrTA** were optimized and their structures are displayed in figure S6. In order to obtain a more realistic structure and to allow the formation of all possible H-bonds a methyl moiety was included after the amide terminal groups. The optimized monomers were used in a second step to generate the corresponding 2D stack layer (Figure 3 and Figure S7).



**Figure S4.** Optimized geometries for monomers A) **oPTA** and B) **oPyrTA**.

The corresponding isolated monomers show a minimum-energy geometry in which the **oPTA** moiety remains almost planar with an angle of  $5.87^\circ$  between terephthaloyl and benzenediamine moieties, whereas a value of  $69.08^\circ$  was obtained for **oPyrTA**. Both molecular structures allow the coexistence of  $\pi$ - $\pi$  and H-bonding intermolecular interactions into the 2D stack layers, with remarkable differences between both oligomer models.

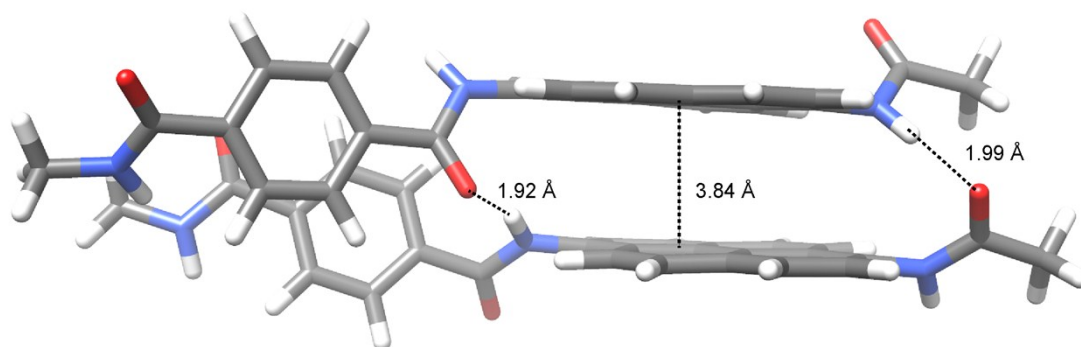


**Figure S5.** Optimized geometry for 2D stacks of 2 units of **PPrTA**.

The stabilization energy values per monomer unit shown in the main text are defined as the energy difference between the unit cell (4 monomer units, 2D stack layer, all interactions present) and the individual monomers (monomers of **oPTA** or **oPyrTA** respectively) at their corresponding optimised geometry:

$$E_{stab} = \frac{(E_{tetramer} - 4 * E_{monomer})}{4}$$

where  $E_{tetramer}$  is the total energy of the 2D stack layers of **oPTA** or **oPyrTA**, and  $E_{monomer}$  is the energy obtained for the monomers (-1047.3304 u.a for **oPTA** and -1430.5526 u.a. for **oPyrTA**) using the optimized geometry depicted in figure S4.

**8) Determination of the average molecular weight of oPTA and oPyrTA by intrinsic viscosity measurement.**

Calculation of the average molecular weight by intrinsic viscosity measurement is a simple method for polymer characterization since the early work of Staudinger in 1930. Oswald method was used for the viscosity measurement, by using an Ubbelohde viscometer at 25 °C in conc. H<sub>2</sub>SO<sub>4</sub> where the flow data was used to calculate the intrinsic viscosity by extrapolating the reduced viscosity to zero concentration. Particularly, by comparing the flow time of the solution with the flow time of the pure solvent relative viscosity, specific viscosity and inherent viscosity were determined. Three different concentrations (0.1, 0.2 and 0.3 dLg<sup>-1</sup>) were used to determine the viscosities of oPTA and oPyrTA

Values of intrinsic viscosity were determined by extrapolating inherent viscosities to zero concentration, obtaining  $[\eta]_{\text{oPTA}} = 50.9 \text{ mlg}^{-1}$  and  $[\eta]_{\text{oPyrTA}} = 80.1 \text{ mlg}^{-1}$ . The molecular weight was calculated using the Mark-Houwink relation:

$$[\eta] = K \cdot M^a \text{ (equation 1)}$$

Where K and a are characteristic parameters for each family of polymers. For aramides  $K = 8 \times 10^{-3} \text{ mlg}^{-1}$  and  $a = 1.09$ .

**Table S1.** Sizes and comparative data for oPTA and oPyrTA obtained from viscosity measurements.

oligomer	Mw <sup>a</sup> (g/mol)	n <sup>b</sup>
oPTA	$3 \times 10^3 \pm 500$	$12 \pm 2$
oPyrTA	$5 \times 10^3 \pm 500$	$13 \pm 3$

a) Average viscosity molecular weight obtained by eq. 1, (b) estimated number of oligomeric units according to Mw<sup>a</sup>.

9) Determination of mass attenuation coefficient by UV-visible and estimation of number of oligomer units.

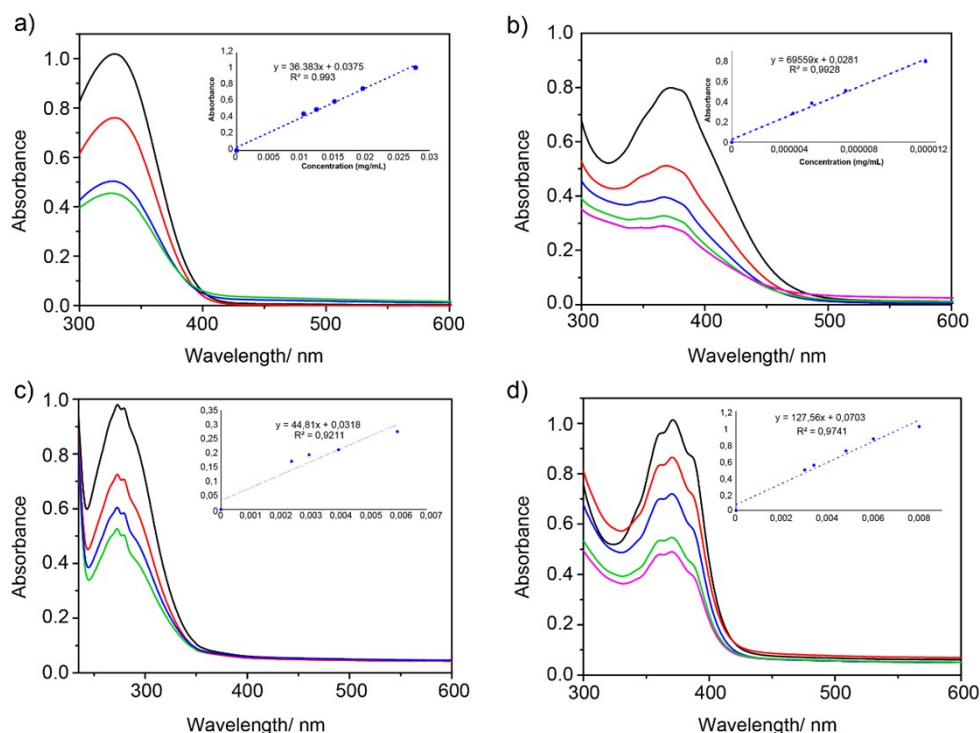


**Figure S6.** UV-vis. measurements and  $\epsilon_{\text{mass}}$  calculation (onsets) for a) **oPTA**, b) **monoPTA**, c) **oPyrTA** and d) **monoPyrTA**.

UV-Vis spectroscopy was carried out to confirm the molecular weight of the aramid oligomers. Lambert-Beer law was used to determine the number of units, assuming that there is no significant electronic interaction between monomers in solution. As mentioned above UV-Vis spectra of oligomers **oPTA**, **oPyrTA** each present an absorption band at 340 nm and 383 nm, respectively. Different concentrations of each were prepared and the absorption data (A) were plotted against concentration (c), from which the mass attenuation coefficient ( $\epsilon_{\text{mass}}$ ) was calculated. Subsequently, the molar attenuation coefficient ( $\epsilon_{\text{molar}}$ ) was determined according to the following equation:  $\epsilon_{\text{molar}} = \epsilon_{\text{mass}} \text{Mw}$ . The same procedure was repeated for monomers **monoPTA** and **monoPyrTA**.

**Table S2:** Calculated MW,  $\epsilon_{\text{mass}}$ ,  $\epsilon_{\text{molar}}$  and number of units (n) for **oPTA**, **oPyrTA**, **monoPTA** and **monoPyrTA**.

Compd.	MW	$\epsilon_{\text{mass}}$ (mL/g.cm)	$\epsilon_{\text{molar}}$ (L/mol.cm)
<b>oPTA</b>	3000	36383	$\epsilon = 109476$
<b>oPyrTA</b>	5000	69559	$\epsilon = 347800$
<b>monoPTA</b>	197.24	44.8	$\epsilon^0 = 8836$
<b>monoPyrTA</b>	321.38	127.6	$\epsilon^0 = 40995$

## 10) Characterization of monomer monoPyrTA

a)  $^1\text{H}$  NMR spectrum (DMSO) of monoPyrTA

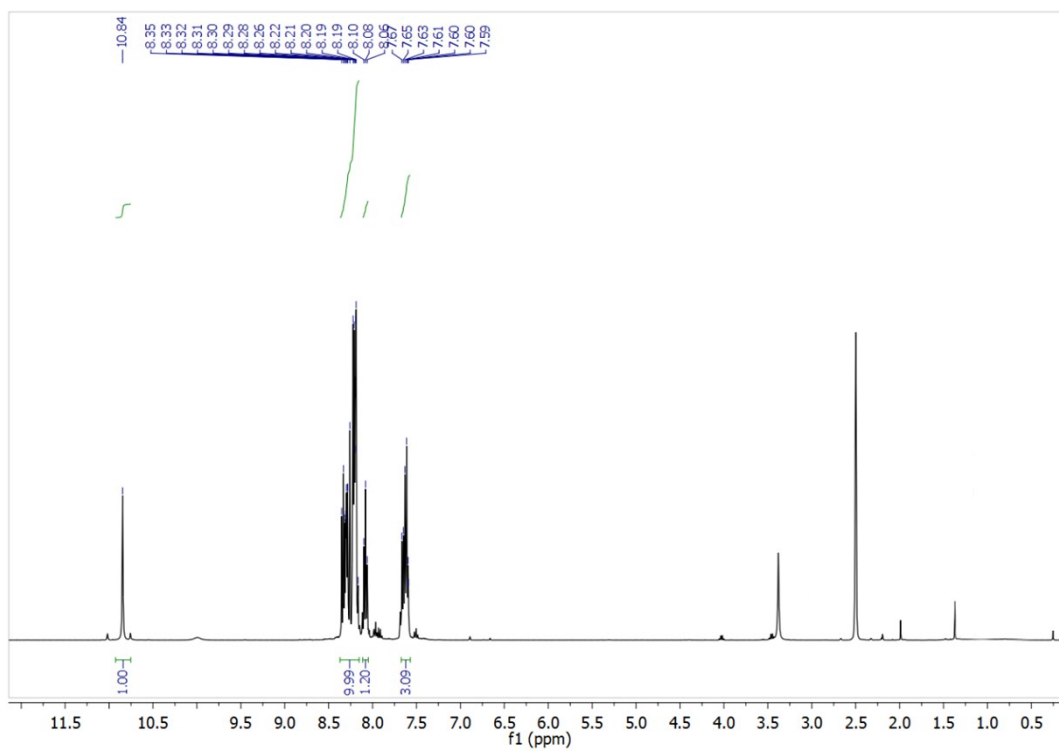


Figure S7

b)  $^{13}\text{C}$  NMR spectrum (DMSO) of monoPyrTA

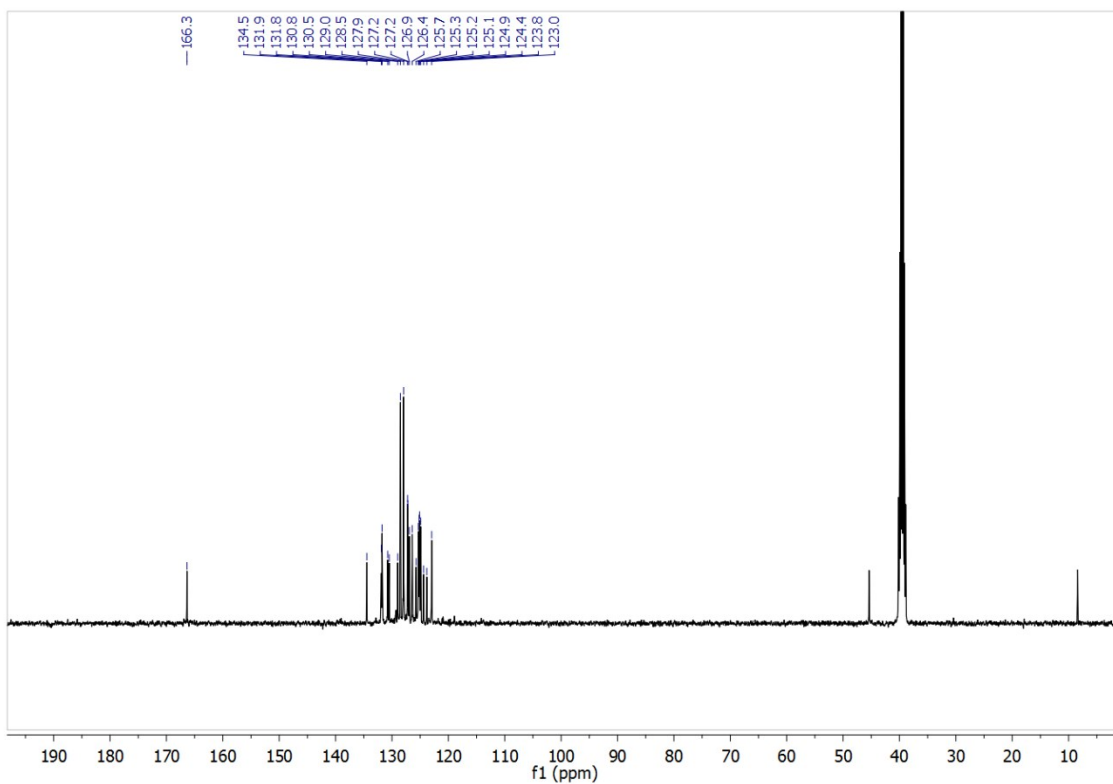


Figure S8.

c) DEPT NMR spectrum (DMSO) of **monoPyrTA**

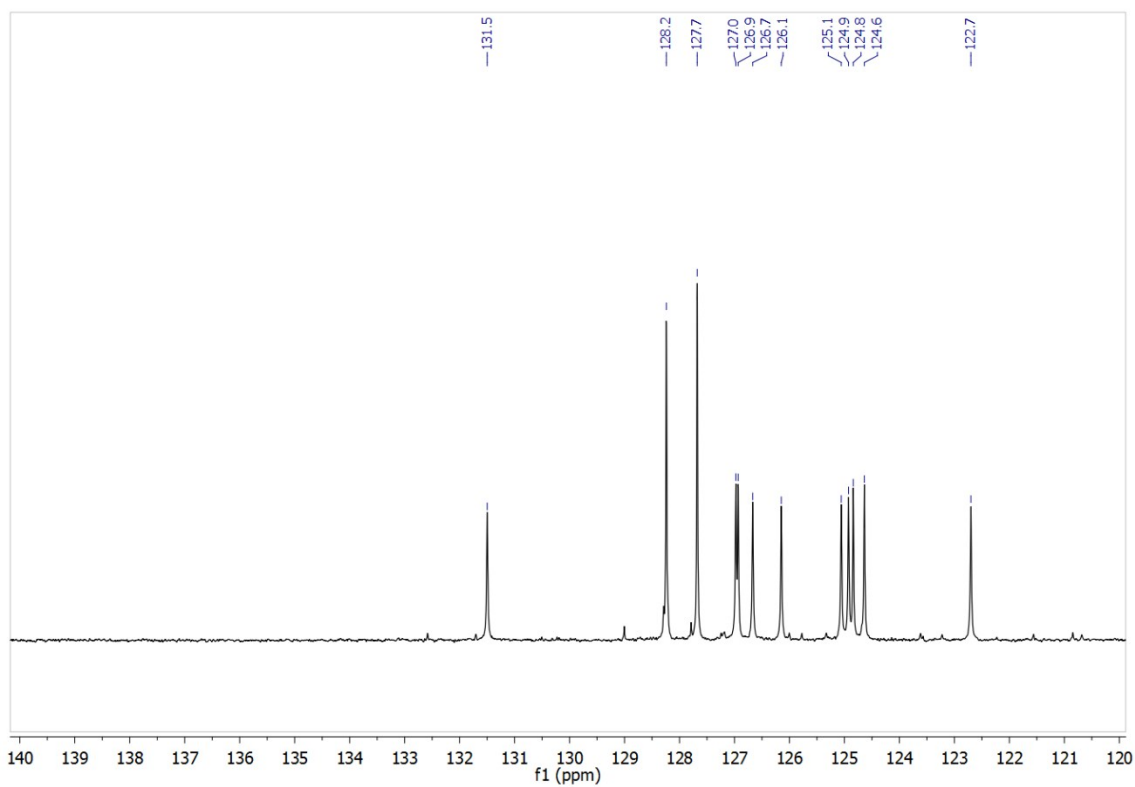
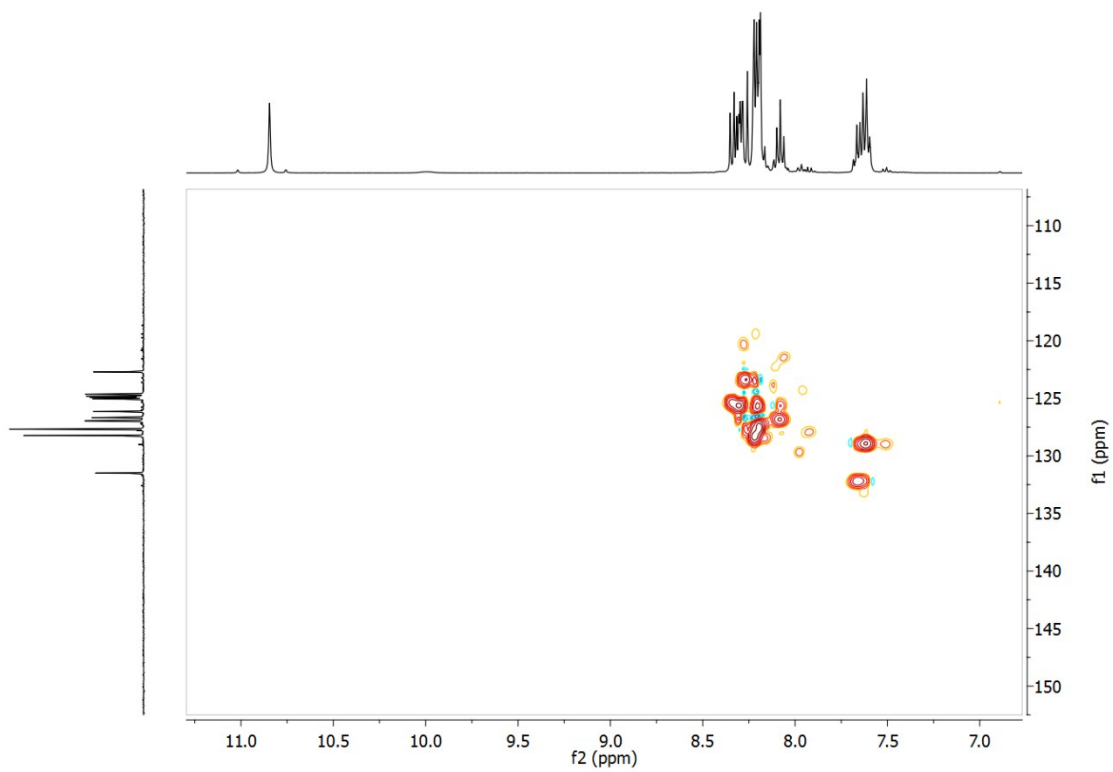


Figure S9

d) HSQC NMR spectrum (DMSO) of **monoPyrTA**



**Figure S10**

e) COSY NMR spectrum (DMSO) of **monoPyrTA**

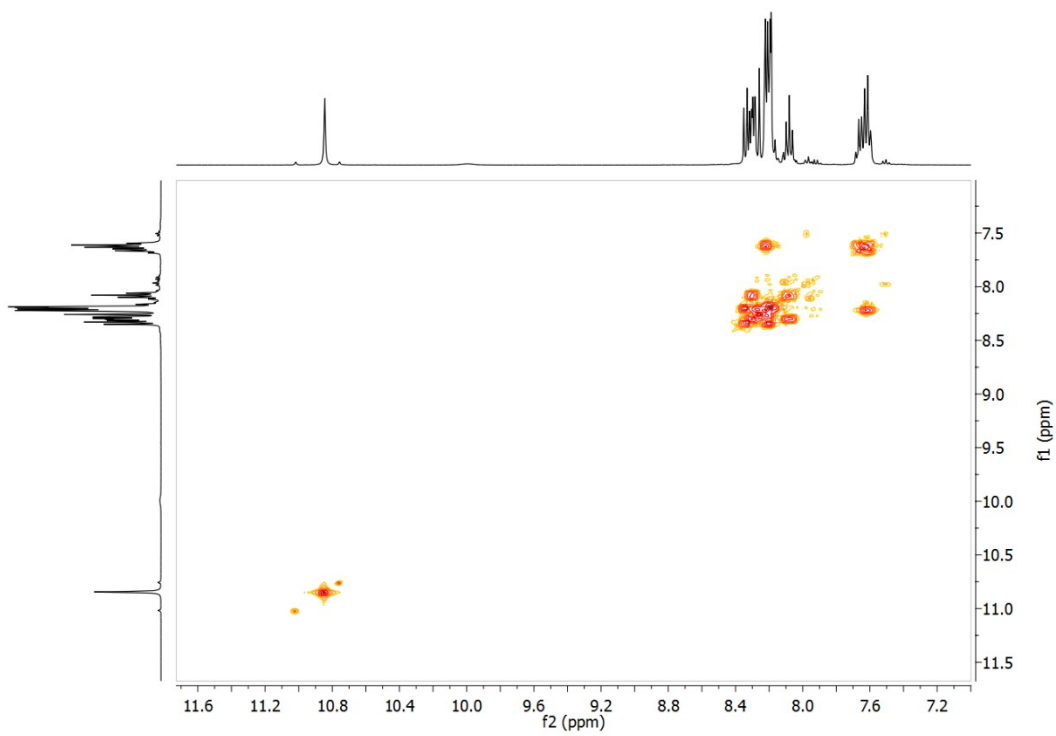


**Figure S11**

f) HMBC NMR spectrum (DMSO) of **monoPyrTA**

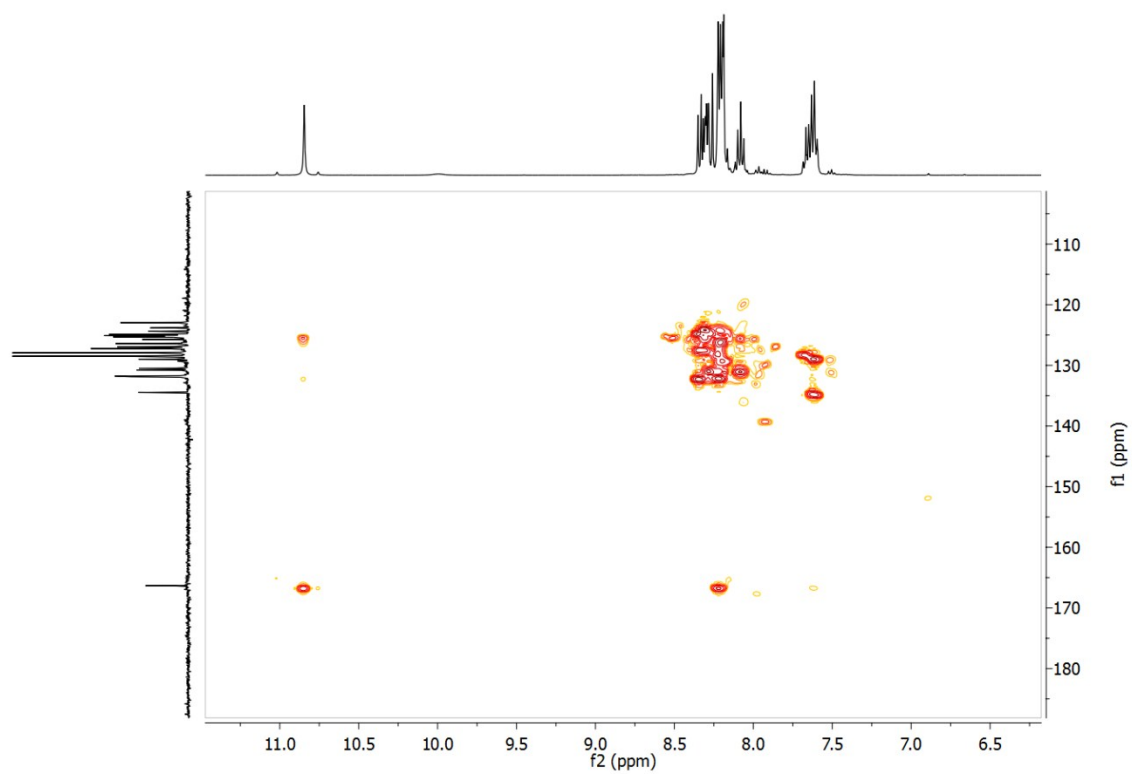


**Figure S12**

g) NOESY NMR spectrum (DMSO) of **monoPyrTA**

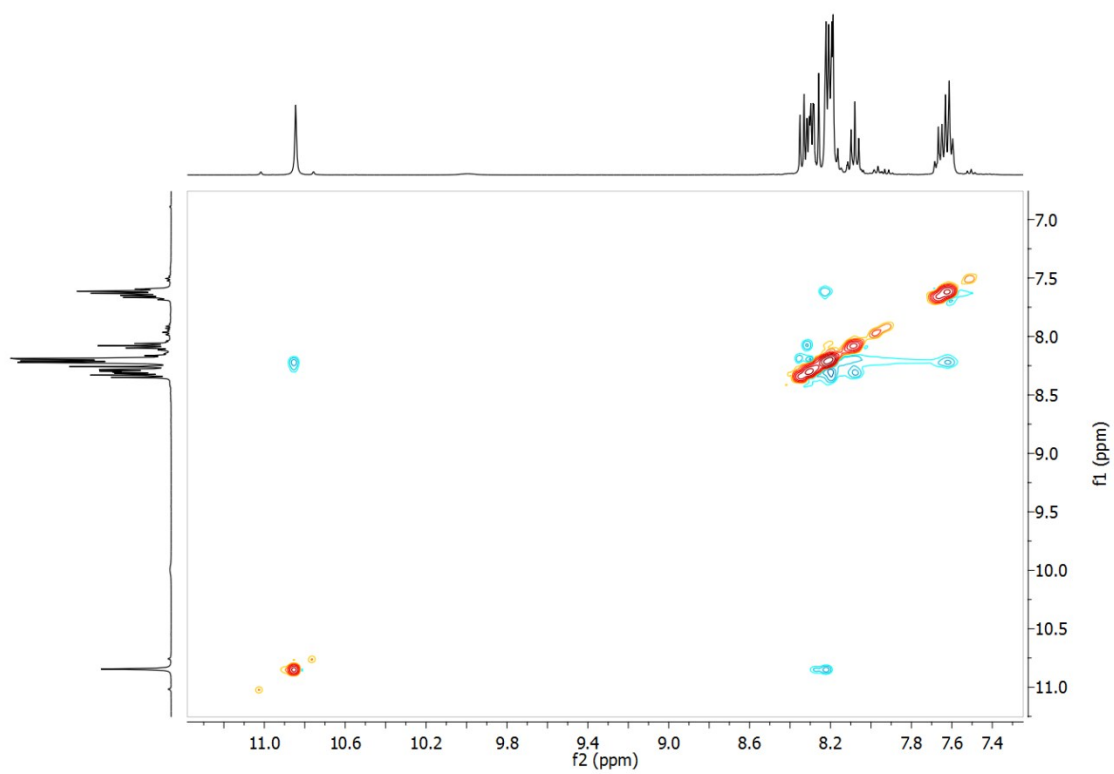


Figure S13

### 11) Synthesis of oPyrTA nanofibers

100 mg KOH (1.8 mmol) was added in 10 mL DMSO ( $c = 0.18 \text{ M}$ ) and stirred for 30 min. Then 11 mg of oPyrTA ( $2 \times 10^{-3} \text{ mmol}$ ) were added and the mixture was stirred for 3 days at R.T. Gradually all the starting oPyrTA solid macroscale fibers were dissolved and oPyrTA nanofibers were obtained as an orange solution.



**Fig S14.** Photo of the solution of oPyrTA nanofibers.

### 12) SEM images of oPyrTA nanofibers

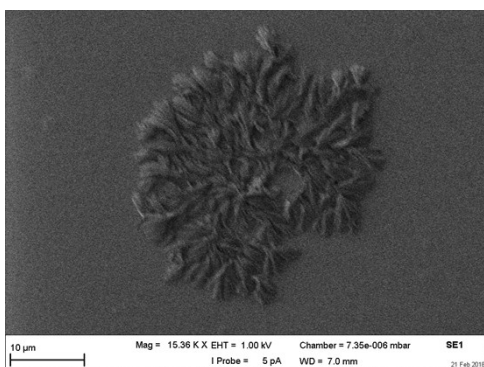


**Fig S15.** SEM image of oPyrTA nanofibers, scale bar: 10  $\mu\text{m}$ .

### 13) Synthesis of oPyrTA nanofilms.

0.05 ml of oPyrTA nanofibers solution was deposited on a glass substrate (26 x 76 mm) which had a paper-spacer in both edges (thickness: 180  $\mu\text{m}$ ) and subsequently sandwiched with another glass substrate. This system, containing oPyrTA nanofibers in a 2D confined-space was then dipped into water and left intact for 3 days. Subsequently, the two glass substrates were carefully separated from each other and left to dry. Then they were dipped in an ethanol solution and sonicated for 5s. Last, they were dipped in an ethanol solution overnight and dried under air.

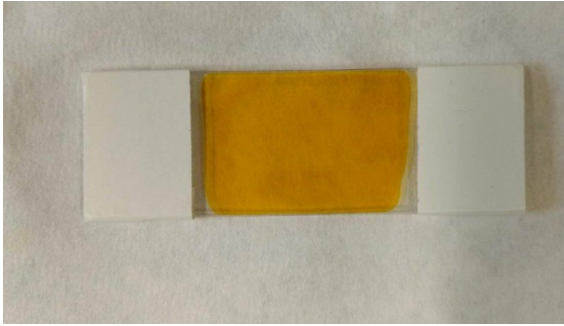


**Fig S16.** Photo of **oPyrTA** nanofibers DMSO solution, sandwiched between two glass substrates separated by 180  $\mu\text{m}$  spacer.

**14) Comparative FT-IR spectra of mono-PyrTA, oPyrTA and oPyrTA nanofilms.**

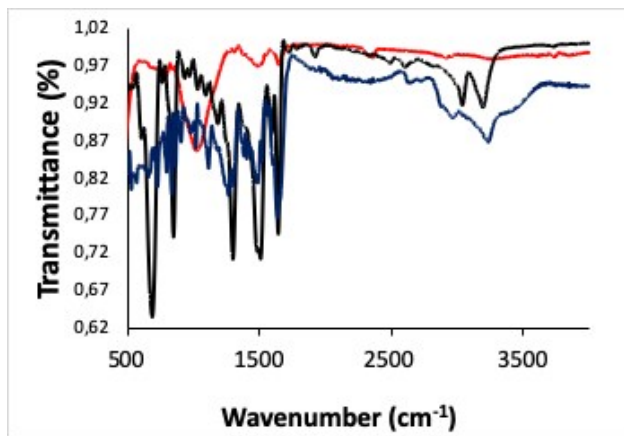


**Figure S17.** FT-IR spectra of **mono-PyrTA** (black), **oPyrTA** (blue) and **oPyrTA** nanofilms (red).

15) Raman spectroscopy of oPyrTA nanofilms.

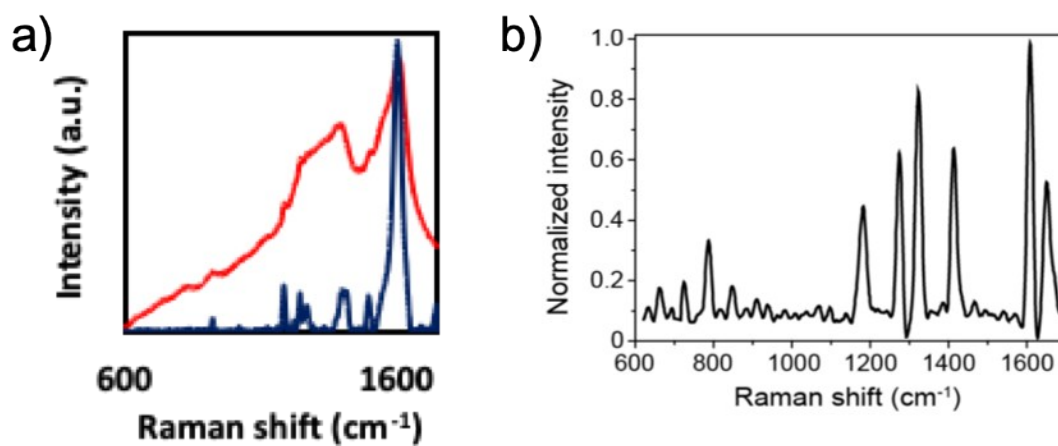


Figure S18. Raman Spectrum of a) oPyrTA (blue) and oPyrTA nanofilms (red), and b) oPTA.

16) TGA analysis of oPyrTA nanofilms.

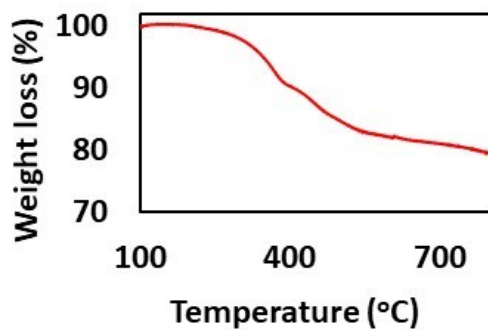


Figure S19. TGA analysis (N<sub>2</sub>, 10°C min<sup>-1</sup>) of oPyrTA nanofilms.

17) SEM/EDS of oPyrTA nanofilms.

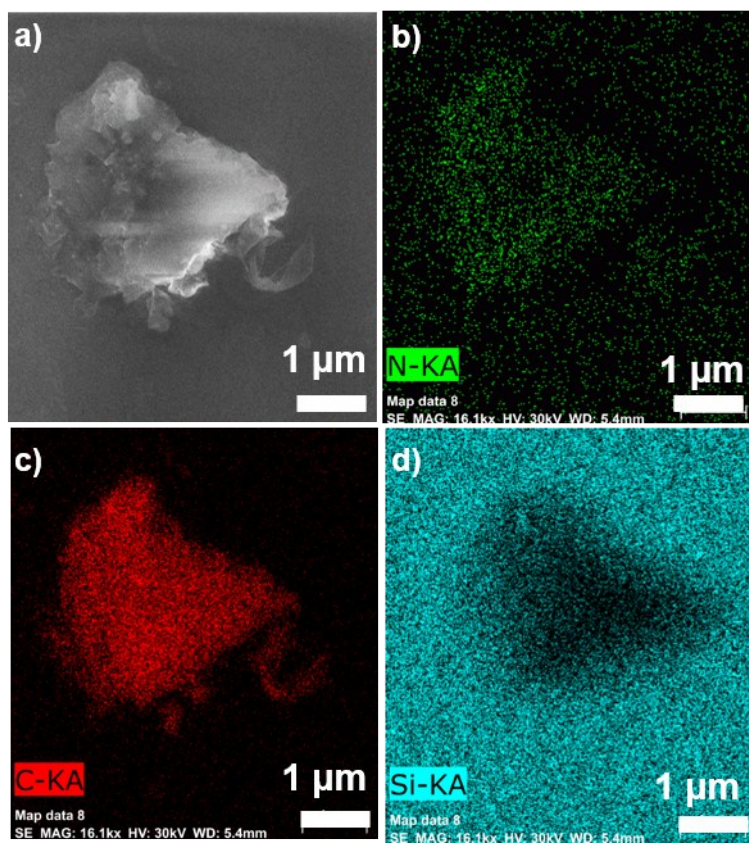
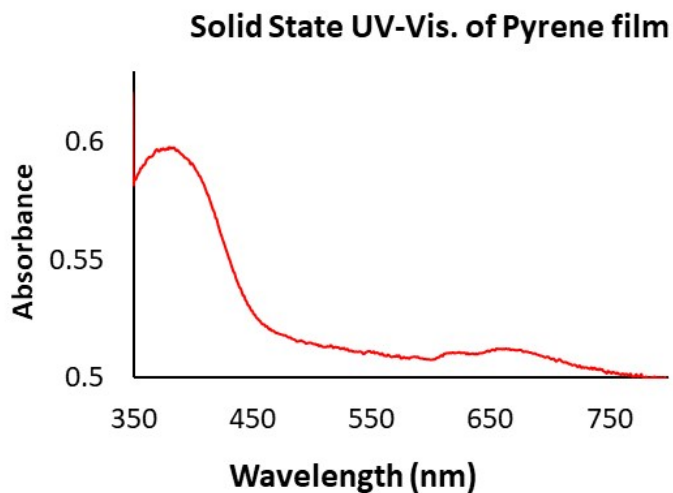


Figure S20. SEM/EDS mapping of a) folded oPyrTA nanofilms for b) N, c) C and d) Si.

### 18) UV/Vis. analysis of oPyrTA nanofilms.



**Figure S21.** UV/Vis. Spectrum of oPyrTA nanofilms. Note the absorption red-shifted feature at 550-750 nm, characteristic of the formation of pyrene excimers. In this case, this feature is more red-shifted than the typical excimer spectrum for pyrene (450-600) probably due to a combination of the molecular structure (the absorption of the pyrenediamine is also redshifted with respect to pyrene) and a scattering contribution. These observations therefore support the efficient p-stacking of the pyrene units in the nanofilm.

### 19) AFM of oPyrTA nanofilms.

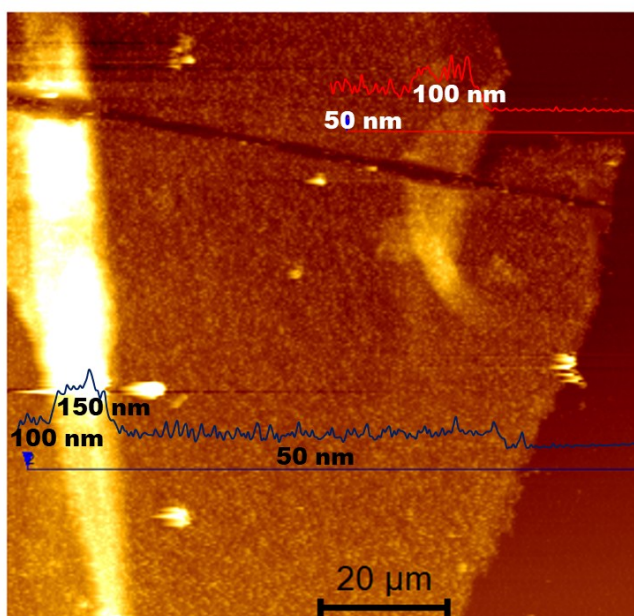


**Figure S22.** AFM topography image of oPyrTA nanofilms, where wrinkles and folds can be also detected.

## 20) Nanoindentation measurements

### a) Oligomers **oPTA** and **oPyrTA**

Nanoindentation testing was performed using a Hysitron TI950 TriboIndenter instrument with a Berkovich geometry diamond indenter. Oligomers **oPTA** and **oPyrTA**, in powder form, were embedded into epoxy resin. Both samples had higher density than epoxy resin, therefore the sample powders were dispersed on the bottom of the mould where resin was poured. Once the epoxy resin was cured at room temperature the face of the piece that contain the sample powders were ground with consecutively finer SiC papers, and finally polished with 3 and 1  $\mu\text{m}$  diamond suspension to reach a surface finish suitable for nanoindentation. The indenter area function was determined using indents on a reference fused silica sample. All data were analysed with the Oliver and Pharr method<sup>1</sup>. The hardness (H) was determined from the peak force ( $P_{\text{max}}$ ) and the projected area of contact, A:

$$H = P_{\text{max}}/A \quad (1)$$

To obtain the elastic modulus, the unloading portion of the load-depth curve was analysed according to a relationship that depends on the contact area:

$$C = \pi^{0.5}/(2E_r A^{0.5}) \quad (2)$$

where C is the contact compliance and  $E_r$  is the reduced modulus defined by

$$1/E_r = (1 - \nu_s^2)/E_s + (1 - \nu_i^2)/E_i \quad (3)$$

where  $\nu_s$  = Poisson's ratio for the sample,  $\nu_i$  = Poisson's ratio for the diamond indenter (0.07),  $E_s$  = Elastic modulus for the sample and  $E_i$  = Young's modulus for the indenter (1141 GPa). Elastic modulus reported here was obtained assuming a Poisson's ratio for the sample of 0.35.

Load-controlled "load-partial-unload" experiments were performed first in order to estimate the added compliance of the resin mount which can cause a significant error in both the measured indentation depth and the contact compliance. The added mount compliance was subtracted from the measured contact compliance (C) and values for modulus corrected accordingly. Indentation tests consisted on quasi-static indentations with load-hold-unload times of 10-5-2 seconds respectively at maximum indentation loads of 1 mN and 5 mN. A total of 15 indentations were carried out on each sample. The substitution of simple phenyl units (in oligomer **oPTA**) by the polycyclic aromatic pyrene moieties (in oligomer **oPyrTA**) improved drastically the elastic modulus and hardness of the oligomeric structure in case of **oPyrTA** compared to oligomer **oPTA**.

### b) **oPyrTA** nanofilms

Nanoindentation testing was carried out on a Hysitron TI950 Triboindenter equipped with either a three-sided pyramidal Berkovich with a tip radius of  $\approx 350$  nm or a cube-corner diamond indenter with a tip radius of  $< 100$  nm. Multiple indentations were performed at different

locations of the film, in load-control mode at different maximum loads, using load-hold-unload cycle times of 30-30-5 s. All data were analysed with the Oliver and Pharr method<sup>1</sup>. To obtain the elastic modulus, the unloading portion of the load-depth curve was analysed according to:

$$E_r = \frac{S\sqrt{\pi}}{2\sqrt{A(h)}} \quad (1)$$

where  $A(h)$  is the contact area, obtained from the tip area function, which was calibrated beforehand from indentations on fused silica,  $S$  is the contact stiffness, and  $E_r$  is the reduced modulus. The hardness ( $H$ ) was determined from the peak load and the projected area of contact  $A(h)$ :

$$H = \frac{F}{A(h)} \quad (2)$$

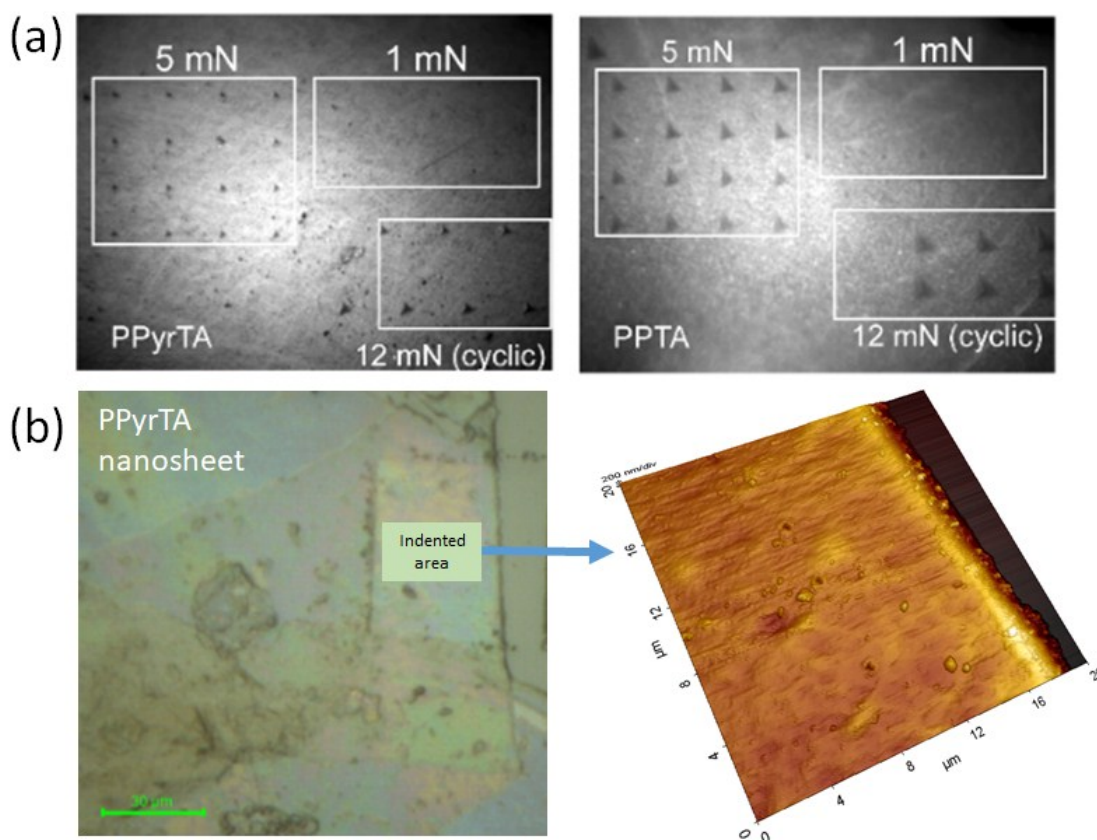


**Figure S23.** (a) Optical images of the nanoindentation experiments at different loads, showing shallower imprints for the harder **oPyrTA** in all cases; (b) Optical (left) and AFM (right) images of one of the indented areas in the **oPyrTA** film. The AFM topographical 3D image shows some of the indentation imprints left by the cube-corner indenter.

An alternative method, referred to as continuous stiffness measurement or *nanoDMA*, can also be used to determine properties of very thin oligomer films. The method is based on

superimposing a small oscillating ac force on the primary dc load on the indenter during indentation and measuring the phase and relative amplitude of the indenter-sample contact response. In this method, described in detail by Oliver & Pharr<sup>3</sup>, the kinematic model of the system, based on a damped harmonic oscillator, is used to relate the stiffness of the contact ( $S$ ), to the phase and amplitude response. The reduced modulus ( $E_r$ ) and hardness ( $H$ ) are then derived as a function of indentation depth ( $h$ ) through the equations of the contact (1-3). The oscillation frequency was set to 200 Hz with variable force amplitude in order to attain oscillation amplitudes of  $\approx 1$ -2 nm. The maximum DC force was  $\approx 400\mu\text{N}$ , in order to reach maximum indentation depths of  $\approx 110$  nm. Indentation tests were carried out using a Berkovich diamond indenter at an indentation strain rate  $\dot{\varepsilon}$  of  $0.1 \text{ s}^{-1}$ , which is given by  $\dot{\varepsilon} = \dot{h}/h$ , where  $\dot{h}$  is the displacement rate. Multiple indentations were made at different sites on the film surface. A topographical AFM image of the indented film is shown in figure S24. The measured film thickness is in the range of 280-320 nm with an average roughness ( $R_a$ ) of  $\approx 15$  nm. Figures 5 a and b shows the reduced modulus and hardness computed from 4 nanoDMA nanoindentation repeats as a function of indentation depth. The plot in figure S25a shows two regions: for depths  $> 25$  nm, the modulus increases due to the effect of the harder glass substrate, while for depths  $< 25$  nm, the reduced modulus reaches a plateau indicating that the modulus correspond to the film, which reaches a value of  $13.1 \pm 0.2$  GPa. The hardness plot of figure S25b obtained from the same indents also reveals a substrate effect, less acute in this case, for depths  $> 50$  nm. The hardness of the films, corresponding to a depth of 30 nm (about 10% of film thickness) is  $0.72 \pm 0.1$  GPa.

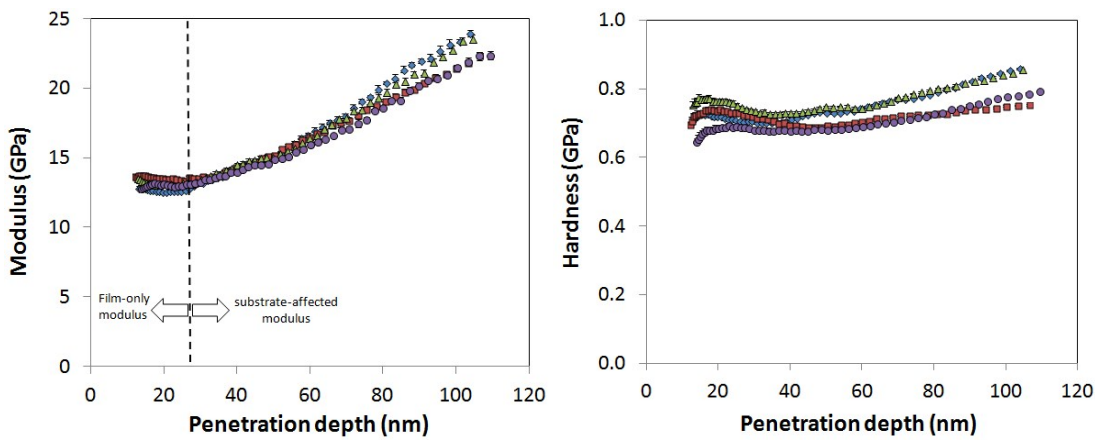


**Figure S24.** (a) Modulus and (b) Hardness as a function of indentation depth.